XIII Congresso Ibérico de Acústica
55º Congreso Español de Acústica
TECNIACÚSTICA 2024
Faro, 11 a 13 setembro 2024

ANALYSIS OF THE DISPERSION RELATIONS AND SOUND TRANSMISSION LOSS IN AN AXIALLY SYMMETRIC ACOUSTIC METAMATERIAL PANEL

D. Ramos[1], L. Godinho[1], P. Amado-Mendes[1], F. Pompoli[2], P. Mareze[3]

[1] University of Coimbra, ISISE, ARISE, Department of Civil Engineering, Coimbra, Portugal
{dtramos@student.dec.uc.pt, lgodinho@dec.uc.pt, pamendes@uc.pt}
[2] Department of Engineering, University of Ferrara, Ferrara, Italy
{ pmpfnc@unife.it}
[3] Acoustical Engineering, Federal University of Santa Maria, Santa Maria, Brazil.
{paulo.mareze@eac.ufsm.br}

Resumo

Nos últimos anos, o novo paradigma dos metamateriais acústicos surgiu como uma estratégia para a manipulação de frentes de onda em regimes de subcomprimento de onda, com um esforço contínuo de várias equipas de investigação no seu desenvolvimento. Pesquisas anteriores evidenciaram a capacidade de sistemas acústicos axialmente simétricos de alcançarem perfeita absorção sonora em banda larga de frequências, possibilitada pelo acoplamento crítico de ressonâncias próximas. Aqui, estendemos ainda mais a ideia de acoplamento axialmente simétrico, criando um meta-painel acústico ventilado que considera a propagação de frentes de onda e suas características de atenuação sonora através de abordagens de fluido equivalente. Assim, o metamaterial acústico proposto é concebido e as suas relações de dispersão são analisadas em função das características geométricas, em situações de ressonâncias simples, dupla e tripla. Deste modo, é realizado um estudo de sensibilidade geométrica, demonstrando como os diferentes parâmetros afetam as relações de dispersão e a respetiva capacidade de transmissão sonora. Demonstra-se que uma interação entre os fenómenos de "band-gap" pode levar a perdas de transmissão sonoras significativas, em torno de 50dB, em frequências sintonizadas. Os resultados obtidos são promissores e ampliam a aplicabilidade destes dispositivos axialmente simétricos no desenvolvimento de novos atenuadores compactos, com aplicação em diferentes contextos de engenharia, incluindo em componentes ou sistemas de edifícios.

Palavras-chave: Metamateriais acústicos, Perdas por transmissão sonora, Relações de dispersão, Sistema axialmente simétrico, Multiplas resonancias.

Abstract

In recent years, the advent of acoustic metamaterials introduced novel strategies for the front wave manipulation on subwavelength regimes which has thus demanded a continuous effort by several researchers. Previous research by the authors has evidenced the capacity of axially-symmetric acoustic systems to achieve perfect absorption in broadband frequencies, enabled by the critical coupling of near-local resonances. Here, we further extend the idea of axially-symmetric coupling by creating a ventilated acoustic metamaterial plate dealing with the front wave propagation and sound attenuation characteristics, making use of dissipative equivalent fluid approaches. This type of acoustic metamaterial is here defined, and the corresponding dispersion relations are analysed as a function of the geometrical characteristics, testing single, dual, and triple resonance cases. Then, a geometrical

sensitivity study is performed, demonstrating how the parameters affect the dispersion relations and the respective transmission capacity; it is demonstrated that an interplay between the bandgap phenomena can induce significant averaged transmission loss values of around 50 dB, at tuned frequencies. The obtained results are promising and expand the applicability of these axially symmetric devices in the development of novel compact attenuators with applications in different engineering contexts, especially in building environments.

Keywords: Acoustic metamaterial, Sound Transmission Loss, dispersion relations, symmetric-axially system, multiple resonance.

PACS no. 43.50.Gf, 43.55.Ti

1 Introduction

In recent years, several attempts have been conducted at the continuous advances in acoustic materials, such as acoustic metamaterials (AMM) [1], exploring novel non-natural physical behaviours. The notorious interest in achieving these effective physical behaviours, characterized by the orderly and locally resonant response, induces effective properties of negative bulk modulus [2] or effective negative density [3] (i.e. single-negative acoustic metamaterials exhibiting), as well as double-negative or negative refractive index acoustic metamaterials [4], resulting from the frequency dependent local resonance mechanism.

The inclusion of a locally resonant inclusion in a host structure leads to a stopband phenomenon within which the propagation of acoustic waves is stopped. These stopbands are generally subdivided considering the stopband mechanisms, i.e. phononic crystals (PCs) [5] and locally resonant metamaterials (LRMs) [6].

As observed in the current literature, focusing the exploration on the bandgap formation induced by local resonances along a host structure [7], theoretical models have been proposed to explore the dispersive relations through periodic-sided-branches resonators mounted in parallel [8]. In contrast, following previously developed works [9], herein, we investigate the dispersive relations of an acoustic metamaterial consisting of axially-symmetric inclusions of local resonators placed on a waveguide with a discontinuity, which have been divided into three groups, i.e. single, dual and triple resonances. In this study, we initially explore the effects of the axially-symmetric interaction between the resonators in an illustrative case with no waveguide discontinuity, evidencing the influence of this strategy on the dispersion of Bloch waves relations.

This article is organized as follows: In section 2, the authors propose the acoustic metamaterial and the respective problem description. Then, in section 3, a discussion is presented, divided as: in subsection 3.1, an illustrative example is presented to discuss the bandgap formation in an axially-symmetric system; in subsection 3.2, the geometrical sensitivity is conducted to assess the influence of the geometric characteristics on the bandgap formation. Finally, the main conclusions are presented in section 4.

2 Design and problem definition

2.1 Design description

Figure 1(a), depicts a 3D printed sample of the axially-symmetric acoustic metamaterial panel. The geometric description of the Helmholtz resonators is delineated in Figure 1(b), consisting of six Helmholtz resonators, laterally displaced around the axis of symmetry of the waveguide with radius r_{w}

and length L, representing the lattice constant of the periodic system along the z-axis, and extended infinitely at the xy-plane within the Cartesian coordinate system (x, y, z). The resonator dimensions, with the neck dimensions specified by $l_{\text{neck}}^{[n]}$ and $w_{\text{neck}}^{[n]}$, representing the length and the width, respectively. The resonant cavity volume, $V_{\text{cav}}^{[n]}$, is computed from $l_{\text{cav}}^{[n]}$and $w_{\text{cav}}^{[n]}$, denoting the length and width of the cavity, respectively. The superscript $[n]$ corresponds to the order of the included resonator. At the circular inner boundary, the cross-sectional shape is defined by the radius r_{t}. Concerning the complex geometrical configuration, three possibilities will be presented: the single, dual and triple configurations. These are defined by the number of group sets and the number of local resonances within each configuration, explained in more detail in the next sections.

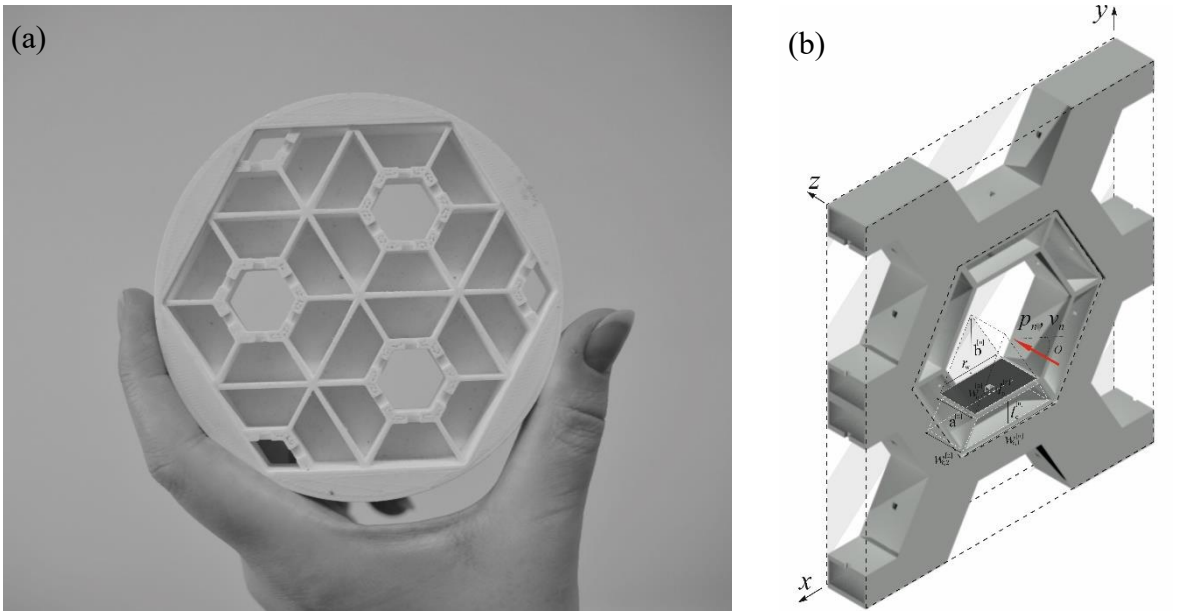

Figure 1 – (a) Photography of the 3D printed sample. (b) Schematic view of a proposed cell array analysed under the acoustic excitation of a plane wave.

2.2 Direct inversion method

To retrieve the dispersion curves of the proposed system, initially we assume the condition of continuity of sound pressure and normal particle acoustic velocity, p and v respectively, in a homogeneous media, through an infinite acoustic system, from the beginning ($x = 0$) to the end of the system ($x = L$), with only the propagation of plane waves, the matrix **T**, can be defined.

$$\mathbf{T}_{\text{total}} \begin{bmatrix} p_1 \\ v_1 \end{bmatrix}_{x=0} = \begin{bmatrix} T_{11} & T_{12} \\ T_{21} & T_{22} \end{bmatrix} \begin{bmatrix} p_2 \\ v_2 \end{bmatrix} = \mathbf{T}_{\text{total}} \begin{bmatrix} p_2 \\ v_2 \end{bmatrix}_{x=L} . \tag{1}$$

Now, consider a periodic lattice and the infinite medium problem along the z-axis, the dispersive relations states that,

$$\begin{Bmatrix} p_1 \\ v_1 \end{Bmatrix} = \mathrm{e}^{-\mathrm{j}\kappa L} \begin{Bmatrix} p_2 \\ v_2 \end{Bmatrix}. \tag{2}$$

By the relation between Eq. 1 and Eq. 2 yields the following equation,

$$(\mathbf{T}_{\text{total}} - \mathrm{e}^{-\mathrm{j}\kappa L}\mathbf{I})\begin{Bmatrix} p_2 \\ v_2 \end{Bmatrix} = 0. \tag{3}$$

The normalized wavenumber is then obtained, kL/π is plotted as a function of frequency, herein is assumed as,

$$k(\omega) = \pm\frac{cos^{-1}(\mathbf{T}_{\text{total}})}{nL} + \frac{2\pi m}{nL}. \tag{4}$$

The passive material condition is satisfied when the imaginary part of $k(\omega)$ is negative. Integer m is chosen to ensure continuity of the real part of $k(\omega)$, and the integer n is the number of cells in the system.

3 Discussion

3.1 An illustrative example of dispersive relations on axially-symmetric inclusions

To analyse the dispersion relation in an axially-symmetric inclusion, initially, we verify the inclusion of a single sided branch Helmholtz resonator. Table 1 summarizes the geometrical dimensions of the Helmholtz resonator, and f_r, the estimated Helmholtz resonance frequency.

Table 1: Geometrical parameters of the single proposition

$w_n^{[n]}$ (mm)	$l_n^{[n]}$ (mm)	$V_c^{[n]}$ (mm^3)	$a^{[n]}$ (mm)	$b^{[n]}$ (mm)	f_r (Hz)
2.4	5	7.4×10^3	25	11.5	565

In Figure 2, the real part of the dispersion curve shows the propagation characteristics of acoustic wavenumber values within the structure, by illustrating the relationship between the angular frequency ω and the normalized wavenumber kL/π of propagating waves. Considering a uniform waveguide with a cross-section radius r_w and periodicity in the z-direction, only the propagation of a fundamental single-mode occurs for angular frequencies $\omega < \pi c_0/L$, with length L in millimetres.

As an illustrative example, the introduction of a lossless resonator ($n_{\text{HR}} = 1$) disrupts the linear behaviour of the waveguide, as can be seen in the dashed blue line, resulting in a local bandgap in the real part around the resonance frequency ($f_{\text{lower},1} < f_{\text{res}} < f_{\text{upper},1}$), with $f_{\text{res}} \approx (c_0/2\pi)\sqrt{S_n/[V_c(2l_n + 1.7r_n)]}$. This phenomenon arises due to the presence of a local resonance induced by the compressive-extensional movement, leading to a negative bulk modulus $K_{eff}(\omega) < 0$, as observed in [10] and previously discussed by [11,12]. At the lower frequency bound, with $f_{\text{lower},1} = f_{\text{res}} = 565$ Hz, the lower limit coincides with the horizontal tangent of the lossless dispersion curve (black dashed line), overestimating the normalized wavenumber to infinite value (Re $(k) \to \infty$). The upper bound is defined as $f_{\text{upper},1} \approx f_{\text{res}}\sqrt{1+\mu} \approx 620$Hz, being the positive root of a simplified wavenumber equation for $k = 0$ [7,13],

$$k = \pm\frac{(2\pi f)}{c_0\sqrt{1+\mu/\left(1-(2\pi f)^2/f_{\text{res}}^2\right)}}, \tag{5}$$

where $\mu = V_{\text{cav}}/(S_w L)$ the volume ratio, i.e. the ratio between the volume enclosed in the resonator cavity and the volume of the unit cell waveguide segment. As a reference, we can observe the relative

bandgap ratio $\Delta f_{\text{lossless},1}/f_{\text{res}} = (f_{\text{upper},1} - f_{\text{lower},1})/f_{\text{res}} = \sqrt{1+\mu} - 1$, which plays a similar role determined by [7,13].

As depicted in Figure 2, for a single inclusion with $n_{\text{HR}} = 1$, the damping effect arising from viscothermal losses becomes evident (solid red line), reflecting the intrinsic frequency dependence of the effective acoustic properties. When defining the bandgap, we observe the first decrease sign in the Re $(kL)/\pi$, or the point where the real part of the in-phase branch bends back, $k_{\text{n},n_{\text{HR}}} = 0.35$, admitting a finite value of the normalized wavenumber with a lower frequency bound $f_{\text{lower},1} \approx 545$ Hz.

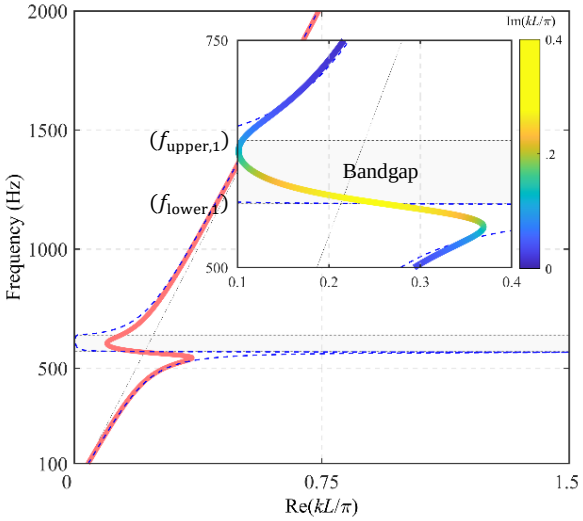

Figure 2 - Dispersion relation of a single lossless and lossy HR. The red solid line represents the real part (propagative) of the dispersion curves. The inset shows the respective single bandgap zone (grey zones), coloured according to Im(kL/π)

In a more complex scenario, Figure 3, the analysis of an axially-symmetric structure composed of the inclusion of a lossy HR with $n_{\text{HR}} = 1,2, \ldots 6$ is conducted. Note that, in Figure 3(a), the real part of the dispersion curve gradually enlarges the relative bandgap ratio when all the resonators tuned at the same resonance frequency $f_{\text{res}} = 565$ Hz. Notably, for $n_{\text{HR}} = 6$, the upper bound corresponds to $f_{\text{lower},6} \approx 820$ Hz, consequently inducing a significant enhancement of the normalized wavenumber node at the propagative part, $k_{\text{n},6} = 0.76$ (see the inset in Figure 3(a)). To illustrate the influence of axially-symmetric resonators on the system, Figure 3(b) presents the attenuative part of the dispersion curve, represented by Im(kL/π), quantifying the attenuation of the acoustic waves as they propagate through a periodic lattice system.

Herein solid lines denote the results obtained from the proposed analytical model utilizing the equivalent fluid approach and the Transfer Matrix Method (TMM), while dashed black lines represent the analytical expressions neglecting viscothermal losses. The square markers represent the data from the FEM simulations, and the circle markers the data from the experimental measurements respectively

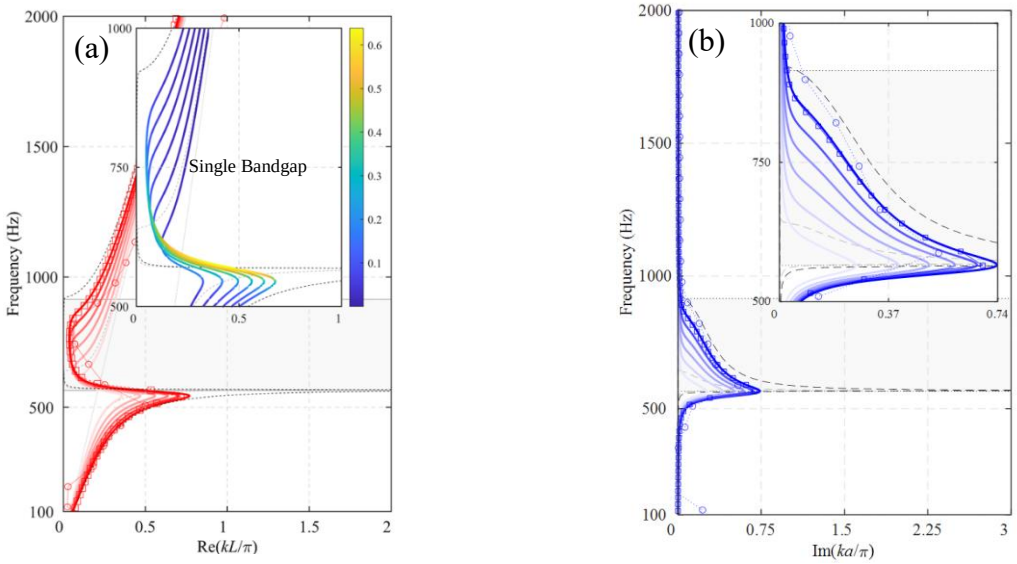

Figure 3 – Dispersion relation of a single resonance metamaterial. (a) The red solid line represents the real part (propagative) of the dispersion relations; (b) The solid blue line represents the imaginary part (attenuated). The solid lines represent the TMM results, the square markers the numerical results, and the circles the experimental results, respectively.

Figure 4 shows the bandgap formation for a dual resonance case, evidencing a second gap. Satisfying the pre-established initial conditions outlined for the single case, in a subsequent scenario, the axially-symmetric mount of different local resonances to investigate complex dispersion relations is proposed through the geometric modification in the width parameter $w_{neck}^{[2]}$= 2.6 mm of the neck's resonator. Thus, in a dual resonance case, we observe the coupling of two near-resonance frequencies, at $f_{dual}^{[1]}$= 565 Hz and $f_{dual}^{[2]}$= 605 Hz, respectively.

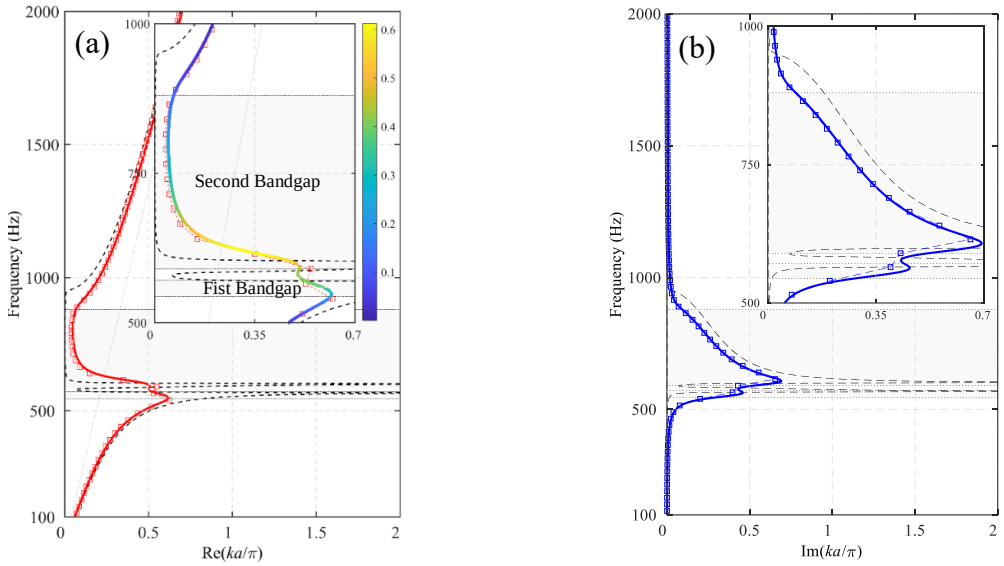

Figure 4 - Dispersion relation of a dual resonance metamaterial. (a) The red solid line represents the real part (propagative) of the dispersion relations; (b) The solid blue line represents the imaginary part (attenuated). The solid lines represent the TMM results, the square markers the numerical results, and the circles the experimental results, respectively.

In a last case, illustrated in Figure 5(a), the onset of the first lower frequency limit of the stopband is observed at $f_{\mathrm{l,triple,1}} = 545$ Hz, and the upper bound at $f_{\mathrm{u,triple,1}} = 570$ Hz delineates the first bandgap. Once the first bandgap is defined, a new bandgap arises, commencing at $f_{\mathrm{l,triple,2}} = 590$ Hz until $f_{\mathrm{u,triple,2}} = 615$ Hz, where an approximation with the dispersion curve of a waveguide is discernible. Finally, a third bandgap originates at $f_{\mathrm{l,triple,3}} = 635$ Hz and its upper-frequency limit at $f_{\mathrm{u,triple,3}} = 900$ Hz.

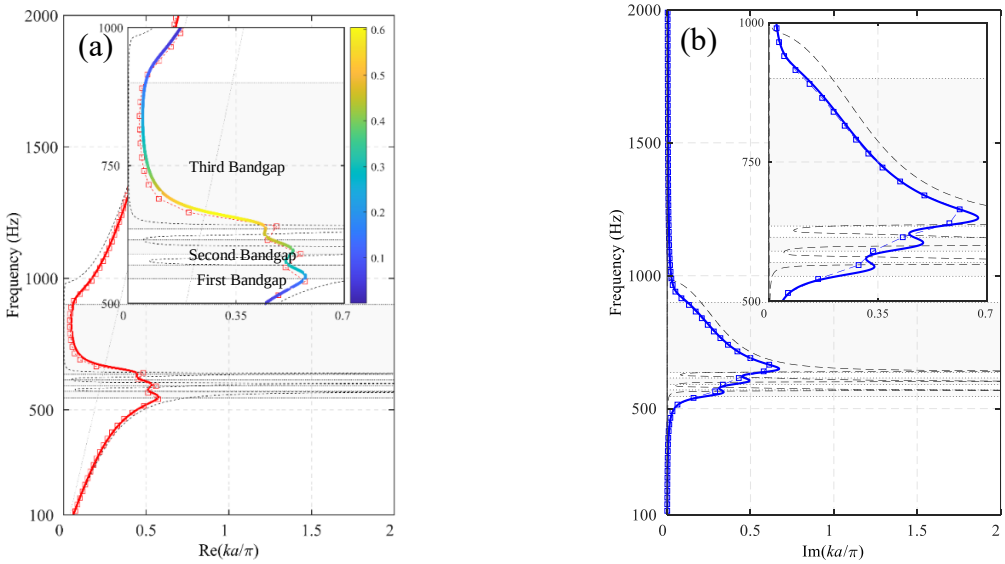

Figure 5 – Dispersion relation of a triple resonance metamaterial. (a) The red solid line represents the real part (propagative) of the dispersion relations; (b) The solid blue line represents the imaginary part (attenuated). The solid lines represent the TMM results, the square markers the numerical results, and the circles the experimental results, respectively.

In summary, as expected in both models, discernible stopbands are induced by the axial-symmetric coupling and due to the geometrical changes. The coupling mechanism induces a phase change which affects the gap formation, with multiple minor bandgaps arising, where the proximity of local resonant frequencies leads to the appearance of an attenuated frequency range.

3.2 Geometrical sensitivity

A sensitivity analysis is performed to investigate the dispersion relation and the sound transmission loss as a function of the geometric parameters, i.e. the filling fraction ϕ_r, $l_{neck}^{[n_{\mathrm{HR}}]}$ and $w_{neck}^{[n_{\mathrm{HR}}]}$. Initially, the geometric parameters, detailed in Table 2, are followed.

Table 2: Geometrical parameters of the panel case

	$w_{neck}^{[n]}$ (mm)	$l_{neck}^{[n]}$ (mm)	$V_{cav}^{[n]}$ (mm^3)	$a^{[n]}$ (mm)	$b^{[n]}$ (mm)	f_r (Hz)
single	2.5	2.5	4.62×10^3	54	7.2	935
dual	3	-	-	-	-	1095
triple	4	-	-	-	-	1390

Figure 6 evidences the formation of the dispersion relations as a function of the filling fraction ratio $\phi_r = \pi {r_w}^2/(\pi {r_t}^2)$, exploring the sound propagation between the outer front panel surface area and the waveguide surface area varying gradually in the filling ratio ϕ_r and the respective percentage rate (10%, 20% and 100%), herein indicated by the different shades of red.
As expected, the results presented in Figure 6, confirm the strict relation between the filling fraction ratio and the sound transmission capacity, as for higher ratios a significant reduction in the attenuation capacity is observed. It is noteworthy that the resonant effect amplifies the inherent attenuation effect arising from the waveguide constriction (with ϕ_r<100%).

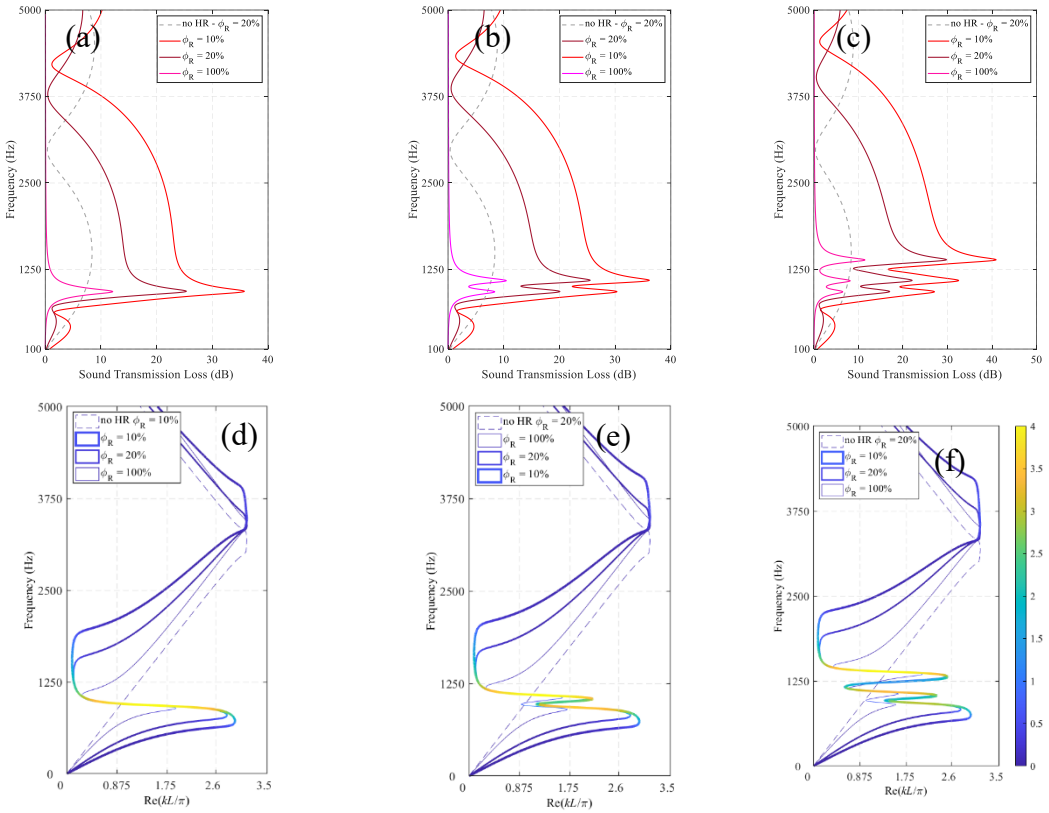

Figure 6 - Influence of the filling ratio on the sound transmission capacity. (a), (b) and (c) the sound transmission losses for the single, dual and triple case, respectively, with ϕ_r = 10%, 20%, and 100%. (a), (b) and (c) the dispersion relation of the single, dual and triple propositions, respectively, coloured according to Im(kL/π).

Figure 7 depicts the induction of the local resonances as a function of the geometrical parameter $l_{\text{neck}}^{[n]}$, taking the variation of the neck length from 0 to 10 mm, and the remaining other parameters fixed with the values presented in Table 2. Figures 7 (a), (b), and (c) present the respective colour maps for each model as a function of $l_{\text{neck}}^{[n]}$. Figure 7 (d) and (e) present respectively, the sound transmission loss and the real part of the dispersion curve, with the bandgaps being easily identified.

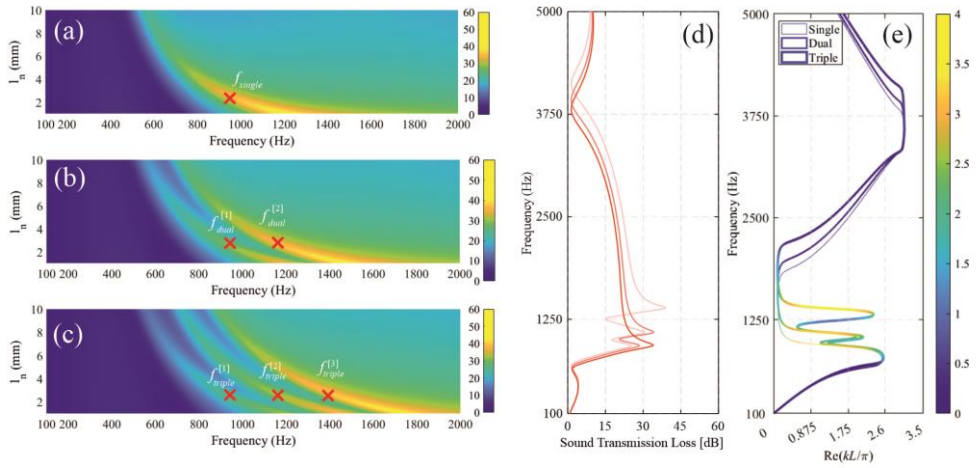

Figure 7- The sensitivity of the sound transmission loss (STL) in function of the geometrical parameters $l_{\mathrm{neck}}^{[\mathrm{n}]}$. (a) Single, (b) dual, and (c) triple resonance cases, respectively; (d) Comparison of the STL for the three propositions. (e) Dispersion curves of the three propositions at the specified geometrical dimension of $l_{\mathrm{neck}}^{[\mathrm{n}]}$, coloured according to $\mathrm{Im}(kL/\pi)$.

Figures 8 (a), (b), and (c) depicts the colourmap as a function of the neck's width $w_{neck}^{[n_{\mathrm{HR}}]}$, for the range from 0 to 10mm, and the remaining other parameters fixed. Setting the respective parameter $w_{neck}^{[n_{\mathrm{HR}}]}$ = 8.5 mm for all resonators, and the respective $l_{neck}^{[1]}$ = 2 mm, $l_{neck}^{[2]}$ = 3 mm, and $l_{neck}^{[3]}$ = 4 mm, and varying the respective value of $V_{cav}^{[n_{\mathrm{HR}}]}$.

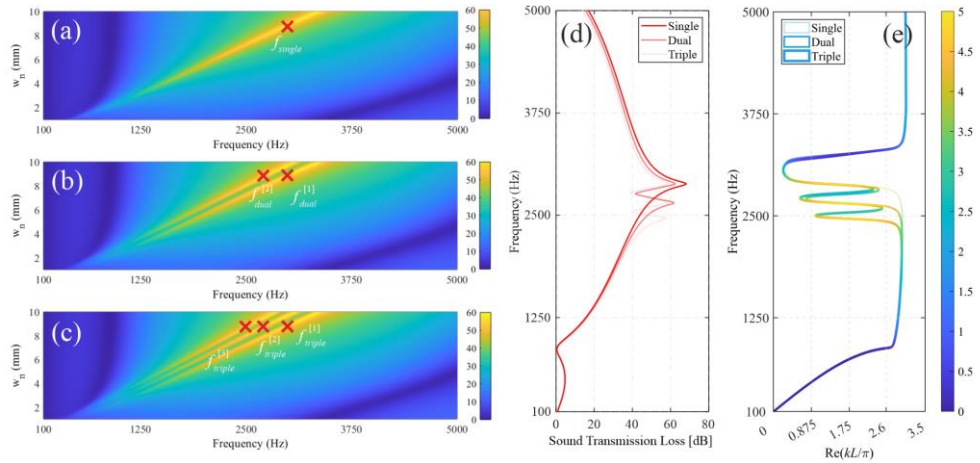

Figure 8 - The sensitivity of the sound transmission loss in function of the geometrical parameters $w_{\mathrm{neck}}^{[\mathrm{n}]}$, for each case, (a) Single, (b) dual, and (c) triple resonance cases. (d) Sound transmission loss spectrum. (e) The real part of the dispersion curves of the three propositions at the specified geometrical dimension of $w_{\mathrm{neck}}^{[\mathrm{n}]}$, coloured according to $\mathrm{Im}(kL/\pi)$.

4 Conclusion

In this work, the complex dispersion curves of an axially-symmetric proposition is investigated, and consequently the sound transmission loss capacity of a proposed acoustic metamaterial. The proposition consists of symmetrical and axial coupling of six Helmholtz resonators, working at single, or multi resonances, inducing the origin of multi bandgaps which consequently enables a high transmission loss capacity at the specified frequency.
The main contributions can be summarised as follows:

- The induction of a local resonance leads a complex dispersion curve, where a local bandgap arises around the resonance frequency ($f_{\mathrm{lower},1} < f_{\mathrm{res}} < f_{\mathrm{upper},6}$).
- Understanding the bandgap formation on the axially-symmetric system, single, dual, and triple resonance models were proposed, and the respective complex dispersion relations in the function of the normalized wavenumber and the sound transmission loss have been evaluated.

Acknowledgements

This work was partly financed by FCT / MCTES through national funds (PIDDAC) under the R&D Unit Institute for Sustainability and Innovation in Structural Engineering (ISISE), under reference UIDB / 04029/2020 (doi.org/10.54499/UIDB/04029/2020), and under the Associate Laboratory Advanced Production and Intelligent Systems ARISE under reference LA/P/0112/2020. This work is financed by national funds through FCT - Foundation for Science and Technology, under grant agreement UI/BD/150864/2021 attributed to the 1st author.

References

[1] Zhang X, Qu Z, Wang H. Engineering Acoustic Metamaterials for Sound Absorption: From Uniform to Gradient Structures. IScience 2020;23:101110. https://doi.org/10.1016/j.isci.2020.101110.

[2] Langfeldt F, Hoppen H, Gleine W. Broadband low-frequency sound transmission loss improvement of double walls with Helmholtz resonators. J Sound Vib 2020;476. https://doi.org/10.1016/j.jsv.2020.115309.

[3] Akl W, Baz A. Active control of the dynamic density of acoustic metamaterials. Appl Acoust 2021;178:108001. https://doi.org/10.1016/j.apacoust.2021.108001.

[4] Liu Y, Xu W, Chen M, Yang T, Wang K, Huang X, et al. Three-dimensional fractal structure with double negative and density-near-zero properties on a subwavelength scale. Mater Des 2020;188:108470. https://doi.org/10.1016/j.matdes.2020.108470.

[5] Ramírez-Solana D, Galiana-Nieves J, Picó R, Redondo J, Sangiorgio V, Graziano AV, et al. Sonic Crystal Noise Barrier with Resonant Cavities for Train Brake Noise Mitigation. Appl Sci 2024;14:2753. https://doi.org/10.3390/app14072753.

[6] Aberkane-Gauthier N, Romero-García V, Lecoq D, Molerón M, Lagarrigue C, Pézerat C. Soft solid subwavelength plates with periodic inclusions: Effects on acoustic Transmission Loss. J Sound Vib 2024;571:118005. https://doi.org/10.1016/j.jsv.2023.118005.

[7] Sugino C, Xia Y, Leadenham S, Ruzzene M, Erturk A. A general theory for bandgap estimation in locally resonant metastructures. J Sound Vib 2017;406:104–23. https://doi.org/10.1016/j.jsv.2017.06.004.

[8] Sugimoto N. Dispersion characteristics of sound waves in a tunnel with an array of Helmholtz resonators. J Acoust Soc Am 1995;97:1446–1459. https://doi.org/10.1017/S0022112092002969.

[9] Ramos D, Pompoli F, Marescotti C, Godinho L, Amado-Mendes P, Mareze P. Modelling the sound transmission properties of a side branch acoustic metamaterial using rigid frame porous model. Proc. 10th Conv. Eur. Acoust. Assoc. Forum Acusticum 2023, Turin, Italy: European Acoustics Association; 2024, p. 4393–6. https://doi.org/10.61782/fa.2023.0296.

[10] Ramos D, Godinho L, Amado-Mendes P, Mareze P. Retrieval method approach for a double-negative acoustic metamaterial composed by discontinued coupling of Helmholtz resonators. 53º Congr. español acústica, XII Congr. Ibérico Acústica, 2022.

[11] Groby JP, Malléjac M, Merkel A, Romero-Garciá V, Tournat V, Torrent D, et al. Analytical modeling of one-dimensional resonant asymmetric and reciprocal acoustic structures as Willis materials. New J Phys 2021;23. https://doi.org/10.1088/1367-2630/abfab0.

[12] Fang N, Xi D, Xu J, Ambati M, Srituravanich W, Sun C, et al. Ultrasonic metamaterials with negative modulus. Nat Mater 2006;5:452–6. https://doi.org/10.1038/nmat1644.

[13] Riva E, Rosa MIN, Guo Y, Ruzzene M. Adiabatic sound transport in acoustic waveguides with time-varying Helmholtz resonators. Front Acoust 2023;1:1–8. https://doi.org/10.3389/facou.2023.1271221.